Applied Physics Letters ARTICLE scitation.org/journal/apl

# Flexible perovskite nanosheet-based photodetectors for ultraviolet communication applications

Cite as: Appl. Phys. Lett. **119**, 251105 (2021); doi: 10.1063/5.0073706
Submitted: 3 October 2021 · Accepted: 6 December 2021 ·
Published Online: 22 December 2021

View Online Export Citation CrossMark

Cheng-Yao Li,[1] Jie He,[1] Yi Zhou,[1] Dong-Xiang Qi,[1] Hao Jing,[1] Jing Su,[2] Ru-Wen Peng,[1,a)] Ren-Hao Fan,[1] Pengcheng Huo,[3] Ting Xu,[3] and Mu Wang[1,4,a)]

## AFFILIATIONS

[1]National Laboratory of Solid State Microstructures, School of Physics, and Collaborative Innovation Center of Advanced Microstructures, Nanjing University, Nanjing 210093, China
[2]School of Physics and Optoelectronic Engineering, Nanjing University of Information Science and Technology, Nanjing 210044, China
[3]National Laboratory of Solid-State Microstructures, College of Engineering and Applied Sciences, and Collaborative Innovation Center of Advanced Microstructures, Nanjing University, Nanjing 210093, China
[4]American Physical Society, Ridge, New York 11961, USA

[a)]**Authors to whom correspondence should be addressed:** rwpeng@nju.edu.cn and muwang@nju.edu.cn

## ABSTRACT

Ultraviolet (UV) photodetection has attracted much attention for applications like monitoring ozone holes and light communication. Although UV photodetectors based on conventional inorganic semiconductors have been widely investigated, fast response devices with high sensitivity remain needed for UV communication systems. This Letter reports on flexible ultrathin methylammonium lead bromide($MAPbBr_3$)-based UV photodetectors. In the UV regime, the response time reaches 3.3/4.0 $\mu$s, and the 3 dB bandwidth is 0.22 MHz. No current degradation is detected after repeated bending cycles, indicating the excellent mechanical flexibility and reliability of flexible high-speed UV photodetectors. Moreover, $MAPbBr_3$ nanosheet-based photodetectors have been integrated into a UV communication system as signal receivers transmitting messages encrypted by international Morse codes. These results reveal the potential of ultrathin perovskite nanosheets in developing flexible optoelectronic devices for UV communications and related applications.



Photodetectors for ultraviolet (UV) detection are paramount for the potential applications in flame monitoring, missile detection, environmental surveillance, etc.[1–4] Optical wireless communication, including communications by UV light, also requires photodetectors possessing fast response speed and high sensitivity to serve as signal receivers in wireless communication systems.[5] Several UV photodetectors with different geometries using wide-bandgap inorganic semiconductors have been explored such as ZnO,[6,7] GaN,[8,9] $Ga_2O_3$,[10,11] and some others.[12–14] However, photodetectors based on these materials often require high temperatures and delicate manufacturing processes and exhibit drawbacks of low sensitivity and slow response speed, which hinder their applications in UV communications and the related fields.

Recently, methylammonium lead halide $MAPbX_3$ (X = Cl, Br, or I), i.e., a hybrid organic-inorganic lead halide perovskite (HOIP) material, has attracted much attention owing to relatively high carrier mobility, long carrier lifetime, and tunable bandgap.[15–20] HOIPs with different geometries can be synthesized by facile solution-processes,[21,22] enabling low-cost, large-area fabrication of lightweight devices. Benefiting from these advantages, HOIPs have emerged as promising candidates for various photoelectrical devices, including light-emitting diodes (LEDs),[23,24] solar cells,[25–28] photodetectors,[29–32] and other photon-to-electron conversion devices.[33–36] Although the development of perovskite-based photodetectors is impeded by the brittle and stiff nature of bulk crystals, the mechanical flexibility of devices can be improved by decreasing the thickness of the active layers to nanometer levels.[37–39] It is possible to fabricate photodetectors with ultrathin HOIPs for flexible signal receivers in optical communications and wearable optoelectronic devices.

This Letter reports on the flexible $MAPbBr_3$ UV photodetectors using ultrathin $MAPbBr_3$ nanosheets as the active layers. A low-cost

quasi-static solution-synthesis of single-crystalline perovskite $MAPbBr_3$ has been employed for growing nanosheets less than 50 nm thick on an atomically smooth mica substrate. The photodetectors made of the nanosheets possess a good responsivity of 24 A/W at wavelength 325 nm, which is comparable to the recently reported perovskite UV photodetector.[40–42] The fast response speed of devices is demonstrated by the rise (fall) time of 3.3 (4.0) $\mu$s and enables a 3 dB bandwidth up to 0.22 MHz in the UV regime. To validate the reliability of the flexible photodetectors, we measure photoelectrical property after repeated bending cycles. No apparent degradation of current is detected. Moreover, we build a UV-light communication system wherein the $MAPbBr_3$ photodetectors serve as UV light signal receivers. Optical messages encoded with the international Morse code can be transmitted when the photodetectors are in either flat or bent states, indicating the promising potential of flexible $MAPbBr_3$ photodetectors for UV communications and wearable devices.

A solution-based quasi-static synthesis[39,43,44] has been employed to grow ultrathin nanosheets of single-crystalline $MAPbBr_3$ on mica substrates. The $MAPbBr_3$ precursor solution is prepared by dissolving $MAPbBr_3$ powder in N, N-dimethylformamide (DMF). The precursor solution is then sandwiched by two freshly cleaved mica sheets. The thin mica sheets serve as flexible substrates and provide an ideal surface in favor of lateral growth to form large crystalline $MAPbBr_3$ sheets due to the atomically flat surface, excellent wettability, and low-chemical activity. The mica-solution-mica assembly is then placed on a hotplate to achieve quasi-static solution growth. Ultrathin single-crystalline $MAPbBr_3$ films grow between the mica sheets. By separating the mica sheets, the single-crystalline $MAPbBr_3$ films can be achieved on the mica substrate. An optical image and atomic force microscopy (AFM) picture of a $MAPbBr_3$ nanosheet grown on mica are illustrated in Fig. 1(a), confirming that the thickness of the nanosheet is less than 50 nm. The roughness of the nanosheet is less than 0.4 nm, indicating that the surface of the nanosheet is ultra-smooth. Scanning electron microscopy (SEM) is used to study the morphology of the $MAPbBr_3$ nanosheets. Figure 1(b) shows that the synthesized nanosheet possesses sharp boundaries and a smooth surface, suggesting the high crystal quality of the nanosheets. The elemental distribution of the perovskite sheet is analyzed with energy-dispersive spectroscopy (EDS). Owing to the poor conductivity of the mica substrate, the EDS analysis and the corresponding SEM images are taken from $MAPbBr_3$ nanosheets grown on the silicon substrate by the same solution-based quasi-static synthesis method. The uniform distribution of the Br and Pb elements in the sample is illustrated in Fig. 1(c), and the ratio of Pb and Br is nearly 1:3, which is consistent with the ratio of 1:3 in $MAPbBr_3$. The crystallinity of the as-grown $MAPbBr_3$ crystals is measured by x-ray diffraction (XRD). Figure 1(d) shows the XRD spectra of the $MAPbBr_3$ samples on a mica substrate and a bare mica substrate. The sharp diffraction peaks at 14.8° and 29.96° correspond to the (001) and (002) planes of $MAPbBr_3$, which are in good agreement with previously reported single-crystalline $MAPbBr_3$.[17,23] In addition, the electron diffraction [Fig. 1(e)] also confirms the single-crystallinity of as-grown films.

We carry out the absorption measurements to verify potential photoelectrical applications of ultrathin $MAPbBr_3$ nanosheets, as depicted in Fig. 1(f). The $MAPbBr_3$ nanosheet exhibits dominant

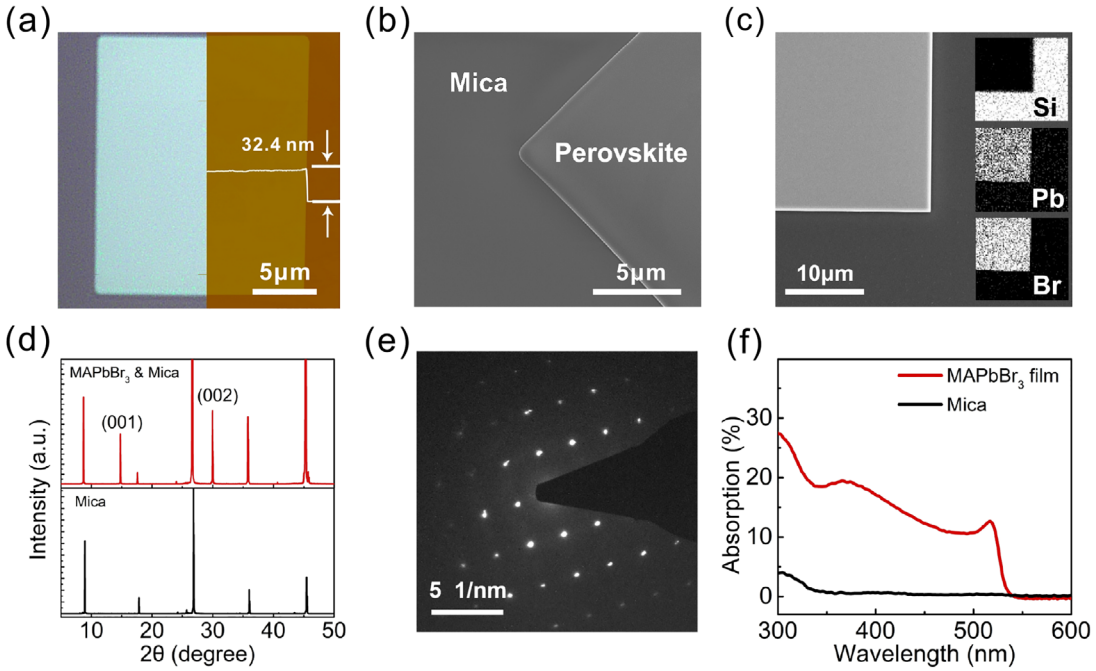


**FIG. 1.** (a) Left: Optical photograph of a grown ultrathin $MAPbBr_3$ nanosheet (half) on mica. Right: AFM image of the corresponding nanosheet (half); inset presents the height profile. (b) SEM image of the nanosheet grown on the mica substrate. (c) SEM image of the nanosheet grown on a silicon substrate; the inset shows EDS analysis images of Br, Pb, and Si elements. (d) XRD patterns of $MAPbBr_3$ samples grown on the mica substrate and bare mica substrate. (e) TEM diffraction pattern of the $MAPbBr_3$ film. (f) Absorption spectra of the nanosheet with the thickness of 24 nm and the mica substrate.

absorption in the UV and visible range with a sharp edge at 536 nm. Notably, the absorption of ultrathin nanosheets in the UV range (<400 nm) is stronger than that in the visible range. Since $MAPbBr_3$ has been widely investigated as a photoactive material in visible-light photodetection,[31,45] it is possible to fabricate $MAPbBr_3$ nanosheet-based photodetectors with good UV photoresponse.

The structure of our ultrathin $MAPbBr_3$ nanosheet-based photodetectors is illustrated in Fig. 2(a). It is similar to the devices in Ref. 39, where the perovskite photodetector was designed to detect visible light only. A pre-patterned mask is used to cover the chosen nanosheet. A layer of Au approximately 40 nm thick is deposited on the nanosheet to fabricate electrodes for the photodetector by thermal evaporation. The separation between the two electrodes is about 4 $\mu$m, as shown in the inset of Fig. 2(a). A program-controlled source meter (Keithley Instruments, 2636 B) is applied to characterize the UV photoresponse of the ultrathin $MAPbBr_3$ photodetector by measuring the current-voltage (I–V) performance under a continuous illumination of 325 nm He-Cd laser with different power densities. Figure 2(b) shows the I-V performance of $MAPbBr_3$ nanosheet-based photodetectors under 325 nm laser illumination with different incident power. It follows that the photocurrent of the $MAPbBr_3$ nanosheet-based photodetector increases with the illumination intensity and reaches 0.52 $\mu$A when the incident power is 4 mW. The on–off ratio at −1 V is calculated over 800 for a dark current of only 0.6 nA. The responsivity ($R$), the critical parameter evaluating the efficiency of photodetectors responding to the incident light, is assessed similarly to that in Ref. 39. The definition of responsivity is $R = \frac{I_{photo} - I_{dark}}{A \times P_{laser}}$, where $I_{photo}$ and $I_{dark}$ are the photocurrent and dark current of the device, respectively, $A$ is the effective area, and $P_{laser}$ is the average power density of the incident laser spot. Figure 2(c) shows the corresponding responsivities as a function of the incident laser power. $R$ reaches 24 A/W when the incident power is 1.2 $\mu$W, which is more than two orders of magnitude higher than that of current commercial Si-based UV sensors. The relationship between the photocurrent and the power of the incident 325 nm laser is also shown in Fig. 2(c), and the linear dynamic range ($LDR$) of the device is calculated as $LDR = 20 \times \log(P_{max}/P_{min})$, where $P_{max}$ and $P_{min}$ are the maximum and minimum incident powers when the photocurrent increases linearly in the logarithmic coordinates. In the entire incident power range (1.2 $\mu$W–4 mW), the photocurrent increases linearly with the incident power, suggesting that the linear dynamic range ($LDR$) of the device is at least 70 dB, which is limited by the output power range of the 325 nm laser light source. In addition, the on–off switching properties of a $MAPbBr_3$ photodetector at a voltage of 1 V are shown in Fig. 2(d). The "on" and "off" conditions occur when the device is under 325 nm laser illumination and in the dark, respectively. The photocurrent and dark current

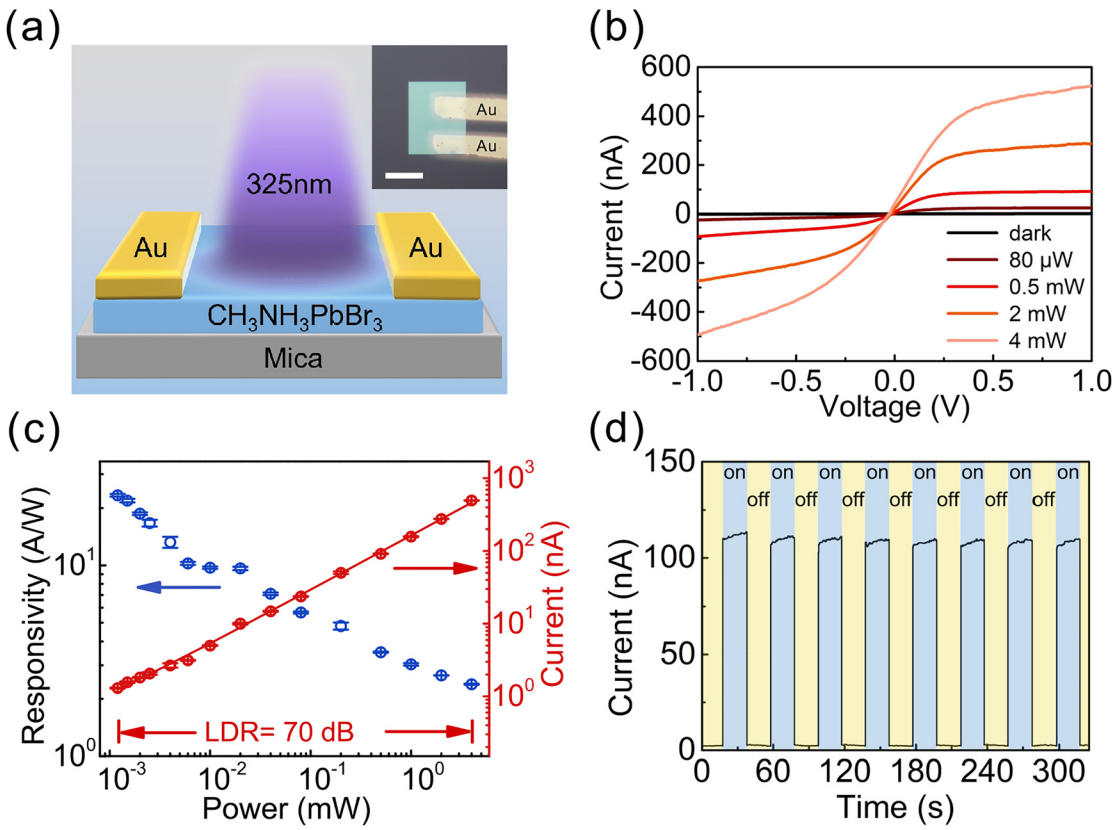


**FIG. 2.** (a) Schematic diagram of the $MAPbBr_3$ photodetector. Inset: the microscopic picture of the photodetector. The scale bar is 10 $\mu$m. (b) I-V performance of $MAPbBr_3$ nanosheet-based photodetectors under 325 nm laser illumination. (c) Responsivity and photocurrent of the photodetector vs incident power at a bias of –1 V. (d) The on/off switching performance of the device.

are repeatable during the cycles from brightness to darkness, demonstrating the stable on-off performance of the device.

To verify that the operation of our devices is not limited to the focused 325 nm laser illumination only, we change the light source to large-area commercial UV LEDs with different wavelengths. I-V and on–off switching measurements are carried out on another similar device under UV LED illumination with a wavelength of 373 nm and a power density of 6.45 mW/cm$^2$. These data are illustrated in Figs. 3(a) and 3(b), respectively. Meanwhile, the responsivity of our devices at different wavelengths has been also evaluated. Under UV LED illumination with the wavelength of 340, 365, and 380 nm, the responsivity reaches around 20, 28, and 38 A/W, respectively. These data confirm that the photodetector can work stably with unfocused UV light illumination at different wavelengths.

For photodetector applications such as light communication, the response time is an important parameter. To characterize the time-resolved response of our $MAPbBr_3$ nanosheet-based photodetectors, we apply a frequency-doubled Ti: sapphire laser connected to an acoustic optical modulator (AOM) and an oscilloscope (Tektronix MDO3012). As shown in Fig. 3(c), the photocurrent increases and decays with the switching on and off of the 385 nm light signal, and the response time for the photocurrent to change from 10% (90%) to 90% (10%) is defined as the rise (fall) time of the device. The rise time and fall time are 3.3 and 4.0 $\mu$s, respectively, under 20 kHz modulated illumination, indicating the fast response speed of $MAPbBr_3$ based photodetectors for UV light detection. The 3 dB bandwidth is another crucial factor in evaluating the response speed of the devices. For our photodetector, the 3 dB bandwidth is defined as the frequency range where the output photocurrent is above half of its maximum under modulated light illumination. The 3 dB bandwidth under 385 nm laser illumination exceeds 0.2 MHz, as shown in Fig. 3(d), implying the potential of the device for UV communications.

The flexibility of photodetectors is also of great importance for wearable device applications. The previous study has demonstrated that, unlike brittle bulk crystals, ultrathin perovskite films possess excellent flexibility.[39] Here, we show the mechanical flexibility of ultrathin $MAPbBr_3$ nanosheet-based UV photodetectors by fitting them to curved surfaces of various radii, as illustrated in Fig. 4(a). Because the side length of the mica is around 12 mm, we use $\theta$, the ratio between the side length of the mica substrate and the radius of the curved surface to characterize the different bent states. The I-V measurement is performed under several values of $\theta$ at ambient conditions as shown in Fig. 4(b). Figure 4(c) presents the photocurrent of a 27 nm thick $MAPbBr_3$ photodetector under a 325 nm laser at a voltage of 1 V as a function of $\theta$. It follows that the photocurrent of the flexible photodetector has no significant loss when the device has been bent from flat to $\theta = 57°$. The normalized photocurrent is illustrated in Fig. 4(d), which indicates the repeatable bending stability of the photodetector.

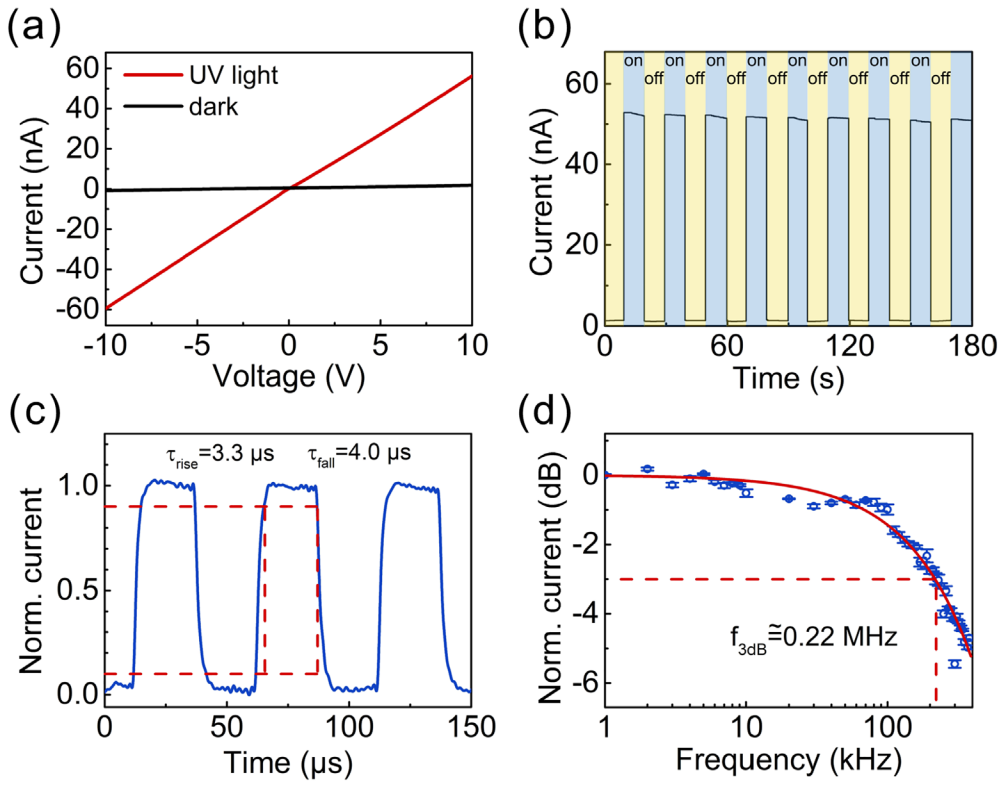


**FIG. 3.** Photodetecting performance under UV LED centered at 373 nm (a) and (b), and time-dependent response under 385 nm illumination (c) and (d). (a) I-V characteristics. (b) On/off switching at a bias of 10 V. (c) Time-resolved photocurrent response at a bias of 1 V with 20 kHz modulation. (d) The normalized response as a function of the input signal frequency at the bias of 1 V, showing the 3 dB bandwidth of the device is about 0.22 MHz.

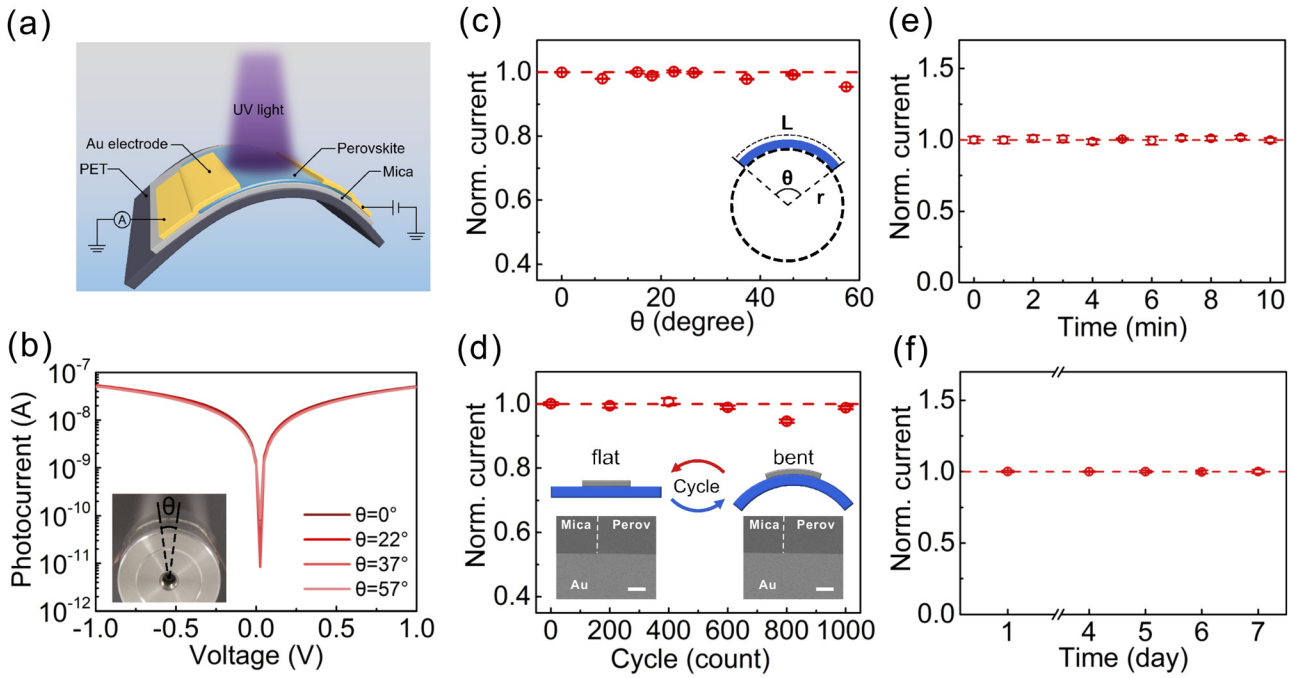


**FIG. 4.** (a) Schematic showing the bending of the flexible $MAPbBr_3$ photodetector. (b) I-V curves of the flexible photodetector at different bending states illuminated by the 325 nm laser with a power of 3 mW. Inset: the cross section of the curved device. (c) The normalized photocurrent vs $\theta$ at a voltage of 1 V. (d) The normalized photocurrent of the flexible device after 1000 repeated bending cycles. Inset: SEM images of several regions in the device before and after the bending. Scale bars are 2 $\mu$m. (e) The normalized photocurrent of the $MAPbBr_3$ device under continuous 325 nm illumination. (f) Stable photocurrent of the device during a week.

Both $MAPbBr_3$ nanosheets and Au electrodes remain unchanged after 1000 bending cycles, as shown in the inset SEM micrographs in Fig. 4(d), and the photocurrent shows no significant degradation. The stability of our devices is also examined. As shown in Fig. 4(e), no obvious photocurrent degradation occurs under continuous illumination with a 325 nm laser. Further by being kept in dry storage but tested in ambient environment during a week, the device presents stable photoelectric response [as shown in Fig. 4(f)], which indicates a long-term stability of this UV photodetector if with encapsulation of PMMA coating. These results suggest that the ultrathin $MAPbBr_3$ photodetector exhibits excellent mechanical flexibility and stability. Compared with the recently-reported flexible UV photodetectors,[4,40,46–50] our device shows remarkably fast response speed and good responsivity at the UV regime (as summarized in Table I), demonstrating the potential in high-speed detections and UV communications.

Taking advantage of the fast response speed, we integrated the $MAPbBr_3$ photodetector into a UV communication system as a signal receiver to convert the input light into an electrical signal. Figure 5(a) shows the experimental setup for UV communications. The input message is first coded in the computer and transformed into high and low voltage levels of different durations by a signal generator. Second, the modulated voltage level is used to activate the AOM to switch a

**TABLE I.** Comparison of the performance of our $MAPbBr_3$ device with reported flexible UV photodetectors.

| Material | Material structure | Thickness of active layer | Responsivity | Rise/fall time | Reference |
|---|---|---|---|---|---|
| $MAPbBr_3$ | Nanosheet | ~35 nm | 24 A/W at 325 nm at 1 V | 3.3/4.0 $\mu$s | This work |
| ZnO QDs/$Zn_2SnO_4$ | Quantum dots decorated nanowires | ⋯ | $>3 \times 10^6$ A/W at 305 nm at 1 V | 47/58 ms | 4 |
| $Ca_2Nb_3O_{10}$ | Nanosheet | 80 nm | 1156 A/W at 270 nm at 1 V | 0.08/5.6 ms | 40 |
| $CH_3NH_3PbCl_3$/ PTAA/ZnO | Quantum dots doped film | 155 nm | 12.27 mA/W at 390 nm at 0 V | 28/- $\mu$s | 46 |
| $CsPbCl_3$ | Nanocrystal | 100 nm | 8.1 A/W at 365 nm at 5 V | 28/31 ms | 47 |
| hBN | Nanosheet | 6–33 nm | 5.022 A/W at 210 nm at 5 V | 200/- ms | 48 |
| p-CuZnS/n-$TiO_2$ | Heterojunction | ⋯ | 640 A/W at ~340 nm at 1 V | <0.2 s/<0.2 s | 49 |
| ZnO/PEDOT:PSS | Heterojunction | 3.82 $\mu$m | 20 mA/W at 325 nm at 0 V | … | 50 |

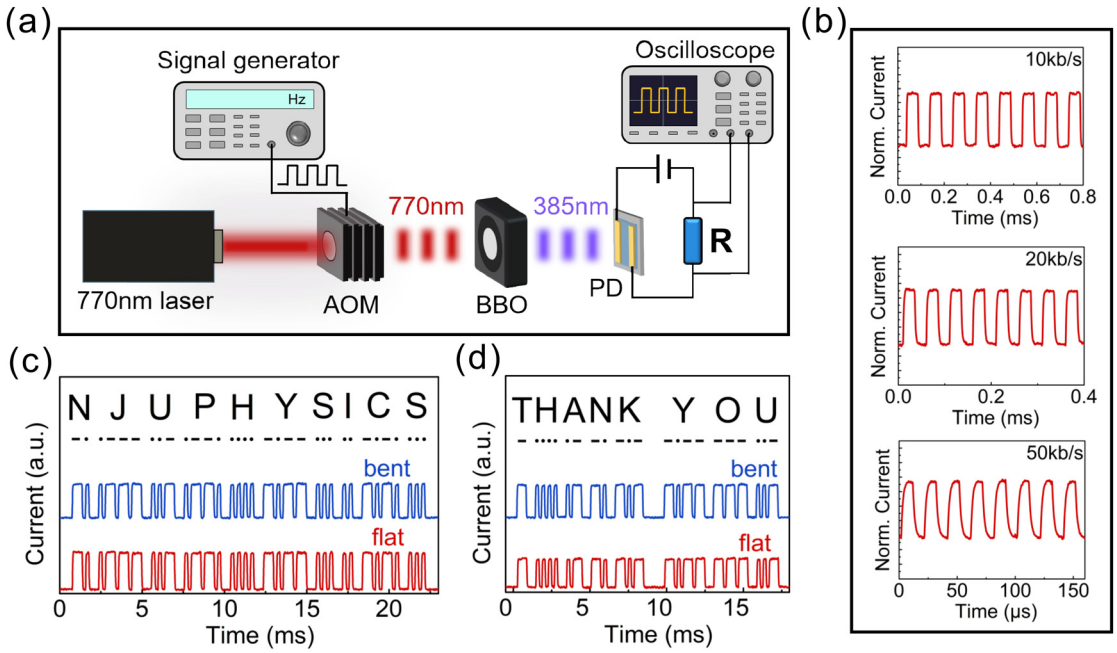


**FIG. 5.** (a) Schematic diagram of the UV communication system based on flexible $MAPbBr_3$ photodetectors. (b) The waveform of digital data received by photodetectors at the transmit rate of 10, 20, and 50 kb/s. (c) The waveforms for "NJUPHYSICS" and (d) "THANK YOU" as the output current signals when the photodetector is in a flat state and a bent state with $\theta = 22°$.

femtosecond-pulsed laser at 770 nm in a specific time sequence corresponding to the input message. Then, the modulated 770 nm light passes through a frequency-doubled crystal and filters to generate a 385 nm light with the same time sequence that the $MAPbBr_3$ photodetector may detect. Finally, the photodetector collects the light signal and converts it into the corresponding electrical response. The current waveform generated by the photodetector is monitored by a load resistor and analyzed by an oscilloscope with an input impedance of 50 MΩ. To evaluate the transmission speed of the system, we apply 50% duty ratio square wave signals with different frequencies to modulate the input light. The corresponding current waveforms from the photodetector are demonstrated in Fig. 5(b), confirming that the system can transmit data at a bit rate of 50 kbps. The system speed can be optimized further by decreasing the load resistance in the circuit. To check the feasibility of text communication, we encrypt the input messages with international Morse code and wirelessly transmit them to the photodetector by modulating 385 nm light. The corresponding current signals are collected and plotted as I-t curves in Fig. 5(c). Three communication states, dot, dash, and silence, are presented by switching on and off the high current with duration differences. The output message "NJUPHYSICS" is obtained after we collect the waveform of the current signal and decode the dot and dash sequence, similar to the one we input into the computer. Furthermore, we demonstrate that the ultrathin $MAPbBr_3$ photodetector can function as a UV signal receiver with good flexibility. As illustrated in Figs. 5(c) and 5(d), the I-t curve generated by the bent photodetector is the same as that of the flat one, and the current sequences are decoded as "NJUPHYSICS" and "THANK YOU."

To summarize, we have grown ultrathin $MAPbBr_3$ nanosheets by a low-cost quasi-static solution-based approach and fabricated flexible $MAPbBr_3$-based UV photodetectors. The photodetectors are demonstrated to have fast response speed in the UV region under ambient conditions. In addition, we exhibit that the ultrathin nanosheet-based UV photodetectors possess excellent mechanical flexibility and robustness with no degradation in the photoresponse during repeated bending cycles. Furthermore, we introduce the $MAPbBr_3$ photodetectors into a UV communication system as flexible signal receivers. The message coded by the international Morse code is transmitted irrespective of whether photodetectors are in the flat or bent states. Our work suggests that the high-speed $MAPbBr_3$ photodetectors can be applied for UV communications and flexible optoelectronic devices in bionics and robotics.

This work was supported by the National Key R&D Program of China (Nos. 2020YFA0211300 and 2017YFA0303702) and the National Natural Science Foundation of China (Grant Nos. 11634005, 61975078, and 11974177).

## AUTHOR DECLARATIONS

### Conflict of Interest

The authors declare no conflicts of interest.

### Author Contributions

C.-Y.L. and J.H. contributed equally to this work.

## DATA AVAILABILITY

The data that support the findings of this study are available from the corresponding authors upon reasonable request.

## REFERENCES


[1]C. Xie, X.-T. Lu, X.-W. Tong, Z.-X. Zhang, F.-X. Liang, L. Liang, L.-B. Luo, and Y.-C. Wu, Adv. Funct. Mater. **29**, 1806006 (2019).
[2]L. Sang, M. Liao, and M. Sumiya, Sensors **13**, 10482 (2013).
[3]P. Cheong, K.-F. Chang, Y.-H. Lai, S.-K. Ho, I.-K. Sou, and K.-W. Tam, IEEE Trans. Ind. Electron. **58**, 5271 (2011).
[4]L. Li, L. Gu, Z. Lou, Z. Fan, and G. Shen, ACS Nano **11**, 4067 (2017).
[5]H. Fang, C. Zheng, L. Wu, Y. Li, J. Cai, M. Hu, X. Fang, R. Ma, Q. Wang, and H. Wang, Adv. Funct. Mater. **29**, 1809013 (2019).
[6]W. Tian, C. Zhang, T. Zhai, S. L. Li, X. Wang, J. Liu, X. Jie, D. Liu, M. Liao, Y. Koide, D. Golberg, and Y. Bando, Adv. Mater. **26**, 3088 (2014).
[7]X.-W. Fu, Z.-M. Liao, Y.-B. Zhou, H.-C. Wu, Y.-Q. Bie, J. Xu, and D.-P. Yu, Appl. Phys. Lett. **100**, 223114 (2012).
[8]A. Gundimeda, S. Krishna, N. Aggarwal, A. Sharma, N. D. Sharma, K. K. Maurya, S. Husale, and G. Gupta, Appl. Phys. Lett. **110**, 103507 (2017).
[9]D. Guo, Y. Su, H. Shi, P. Li, N. Zhao, J. Ye, S. Wang, A. Liu, Z. Chen, C. Li, and W. Tang, ACS Nano **12**, 12827 (2018).
[10]D. Zhang, W. Zheng, R. C. Lin, T. T. Li, Z. J. Zhang, and F. Huang, J. Alloys Compd. **735**, 150 (2018).
[11]M. Ai, D. Guo, Y. Qu, W. Cui, Z. Wu, P. Li, L. Li, and W. Tang, J. Alloys Compd. **692**, 634 (2017).
[12]X. Fang, L. Hu, K. Huo, B. Gao, L. Zhao, M. Liao, P. K. Chu, Y. Bando, and D. Golberg, Adv. Funct. Mater. **21**, 3907 (2011).
[13]J. Chu, F. Wang, L. Yin, L. Lei, C. Yan, F. Wang, Y. Wen, Z. Wang, C. Jiang, L. Feng, J. Xiong, Y. Li, and J. He, Adv. Funct. Mater. **27**, 1701342 (2017).
[14]J. Xu, W. Yang, H. Chen, L. Zheng, M. Hu, Y. Li, and X. Fang, J. Mater. Chem. C **6**, 3334 (2018).
[15]C. M. Sutter-Fella, Y. Li, M. Amani, J. W. Ager III, F. M. Toma, E. Yablonovitch, I. D. Sharp, and A. Javey, Nano Lett. **16**, 800 (2016).
[16]M. R. Filip, G. E. Eperon, H. J. Snaith, and F. Giustino, Nat. Commun. **5**, 5757 (2014).
[17]D. Wang, W. B. Shi, H. Jing, C. Yin, Y. Zhu, J. Su, G. B. Ma, R. Peng, X. Wang, and M. Wang, Opt. Express **26**, 27504 (2018).
[18]D. W. de Quilettes, S. M. Vorpahl, S. D. Stranks, H. Nagaoka, G. E. Eperon, M. E. Ziffer, H. J. Snaith, and D. S. Ginger, Science **348**, 683 (2015).
[19]Q. Dong, Y. Fang, Y. Shao, P. Mulligan, J. Qiu, L. Cao, and J. Huang, Science **347**, 967 (2015).
[20]G. Xing, N. Mathews, S. Sun, S. S. Lim, Y. M. Lam, M. Grätzel, S. Mhaisalkar, and T. C. Sum, Science **342**, 344 (2013).
[21]H. Huang, J. Raith, S. V. Kershaw, S. Kalytchuk, O. Tomanec, L. Jing, A. S. Susha, R. Zboril, and A. L. Rogach, Nat. Commun. **8**, 996 (2017).
[22]Z. Xiao, C. Bi, Y. Shao, Q. Dong, Q. Wang, Y. Yuan, C. Wang, Y. Gao, and J. Huang, Energy Environ. Sci. **7**, 2619 (2014).
[23]Z. Xiao, R. A. Kerner, L. Zhao, N. L. Tran, K. M. Lee, T.-W. Koh, G. D. Scholes, and B. P. Rand, Nat. Photonics **11**, 108 (2017).
[24]Y.-H. Kim, H. Cho, J. H. Heo, T.-S. Kim, N. Myoung, C.-L. Lee, S. H. Im, and T.-W. Lee, Adv. Mater. **27**, 1248 (2015).
[25]H. Tan, A. Jain, O. Voznyy, X. Lan, F. P. G. de Arquer, J. Z. Fan, R. Quintero-Bermudez, M. Yuan, B. Zhang, Y. Zhao, F. Fan, P. Li, L. N. Quan, Y. Zhao, Z.-H. Lu, Z. Yang, S. Hoogland, and E. H. Sargent, Science **355**, 722 (2017).
[26]D. Bi, C. Yi, J. Luo, J.-D. Décoppet, F. Zhang, S. M. Zakeeruddin, X. Li, A. Hagfeldt, and M. Grätzel, Nat. Energy **1**, 16142 (2016).
[27]D. Luo, W. Yang, Z. Wang, A. Sadhanala, Q. Hu, R. Su, R. Shivanna, G. F. Trindade, J. F. Watts, Z. Xu, T. Liu, K. Chen, F. Ye, P. Wu, L. Zhao, J. Wu, Y. Tu, Y. Zhang, X. Yang, W. Zhang, R. H. Friend, Q. Gong, H. J. Snaith, and R. Zhu, Science **360**, 1442 (2018).
[28]W. Nie, H. Tsai, R. Asadpour, J.-C. Blancon, A. J. Neukirch, G. Gupta, J. J. Crochet, M. Chhowalla, S. Tretiak, M. A. Alam, H.-L. Wang, and A. D. Mohite, Science **347**, 522 (2015).
[29]L. Dou, Y. M. Yang, J. You, Z. Hong, W. H. Chang, G. Li, and Y. Yang, Nat. Commun. **5**, 5404 (2014).
[30]Y. Lee, J. Kwon, E. Hwang, C. H. Ra, W. J. Yoo, J. H. Ahn, J. H. Park, and J. H. Cho, Adv. Mater. **27**, 41 (2015).
[31]Z. Yang, Y. Deng, X. Zhang, S. Wang, H. Chen, S. Yang, J. Khurgin, N. X. Fang, X. Zhang, and R. Ma, Adv. Mater. **30**, 1704333 (2018).
[32]C. Li, H. Wang, F. Wang, T. Li, M. Xu, H. Wang, Z. Wang, X. Zhan, W. Hu, and L. Shen, Light: Sci. Appl. **9**, 31 (2020).
[33]W. Yu, F. Li, L. Yu, M. R. Niazi, Y. Zou, D. Corzo, A. Basu, C. Ma, S. Dey, M. L. Tietze, U. Buttner, X. Wang, Z. Wang, M. N. Hedhili, C. Guo, T. Wu, and A. Amassian, Nat. Commun. **9**, 5354 (2018).
[34]Q. Zhang, Q. Shang, R. Su, T. Thu Ha Do, and Q. Xiong, Nano Lett. **21**, 1903 (2021).
[35]X. Xu, W. Deng, X. Zhang, L. Huang, W. Wang, R. Jia, D. Wu, X. Zhang, J. Jie, and S. T. Lee, ACS Nano **13**, 5910 (2019).
[36]H. Jing, Y. Zhu, R.-W. Peng, C.-Y. Li, B. Xiong, Z. Wang, Y. Liu, and M. Wang, Nanophotonics **9**, 3323 (2020).
[37]H. Deng, X. Yang, D. Dong, B. Li, D. Yang, S. Yuan, K. Qiao, Y. B. Cheng, J. Tang, and H. Song, Nano Lett. **15**, 7963 (2015).
[38]W. Hu, W. Huang, S. Yang, X. Wang, Z. Jiang, X. Zhu, H. Zhou, H. Liu, Q. Zhang, X. Zhuang, J. Yang, D. H. Kim, and A. Pan, Adv. Mater. **29**, 1703256 (2017).
[39]H. Jing, R. Peng, R. M. Ma, J. He, Y. Zhou, Z. Yang, C. Y. Li, Y. Liu, X. Guo, Y. Zhu, D. Wang, J. Su, C. Sun, W. Bao, and M. Wang, Nano Lett. **20**, 7144 (2020).
[40]Y. Zhang, S. Li, Z. Li, H. Liu, X. Liu, J. Chen, and X. Fang, Nano Lett. **21**, 382 (2021).
[41]Z. Cheng, K. Liu, J. Yang, X. Chen, X. Xie, B. Li, Z. Zhang, L. Liu, C. Shan, and D. Shen, ACS Appl. Mater. Interfaces **11**, 34144 (2019).
[42]Z. Chen, C. Li, A. A. Zhumekenov, X. Zheng, C. Yang, H. Yang, Y. He, B. Turedi, O. F. Mohammed, L. Shen, and O. M. Bakr, Adv. Opt. Mater. **7**, 1900506 (2019).
[43]M. Wang, S. Zhong, X.-B. Yin, J.-M. Zhu, R.-W. Peng, Y. Wang, K.-Q. Zhang, and N.-B. Ming, Phys. Rev. Lett. **86**, 3827 (2001).
[44]B. Zhang, Y.-Y. Weng, X.-P. Huang, M. Wang, R.-W. Peng, N.-B. Ming, B. Yang, N. Lu, and L. Chi, Adv. Mater. **21**, 3576 (2009).
[45]B. Du, W. Yang, Q. Jiang, H. Shan, D. Luo, B. Li, W. Tang, F. Lin, B. Shen, Q. Gong, X. Zhu, R. Zhu, and Z. Fang, Adv. Opt. Mater. **6**, 1701271 (2018).
[46]L. Cui, J. Peng, W. Li, Y. Xu, M. Zheng, and Q. Lin, Phys. Status Solidi RRL **14**, 1900653 (2020).
[47]D. Li, D. Zhou, W. Xu, X. Chen, G. Pan, X. Zhou, N. Ding, and H. Song, Adv. Funct. Mater. **28**, 1804429 (2018).
[48]S. Veeralingam, L. Durai, P. Yadav, and S. Badhulika, ACS Appl. Electron. Mater. **3**, 1162 (2021).
[49]X. Xu, J. Chen, S. Cai, Z. Long, Y. Zhang, L. Su, S. He, C. Tang, P. Liu, H. Peng, and X. Fang, Adv. Mater. **30**, 1803165 (2018).
[50]M.-S. Tsai, T.-L. Shen, H.-M. Wu, Y.-M. Liao, Y.-K. Liao, W.-Y. Lee, H.-C. Kuo, Y.-C. Lai, and Y.-F. Chen, ACS Appl. Mater. Interfaces **12**, 9755 (2020).